Hierarchical Control Strategy for Fuel Cell-Battery Shipboard Power System Utilizing a Modular Control Architecture

Kopka, Timon; Löffler, Charlotte; Coraddu, Andrea; Polinder, Henk

Citation (APA)
Kopka, T., Löffler, C., Coraddu, A., & Polinder, H. (2024). Hierarchical Control Strategy for Fuel Cell-Battery Shipboard Power System Utilizing a Modular Control Architecture. In *Proceedings of the IEEE Transportation Electrification Conference and Expo, Asia-Pacific, ITEC Asia-Pacific 2023* IEEE. https://doi.org/10.1109/ITECAsia-Pacific59272.2023.10372342

Important note
To cite this publication, please use the final published version (if applicable).
Please check the document version above.

Hierarchical Control Strategy for Fuel Cell-Battery Shipboard Power System Utilizing a Modular Control Architecture

1st Timon Kopka
Maritime and Transport Technology
Delft University of Technology
Delft, Netherlands
t.kopka@tudelft.nl

2nd Charlotte Löffler
Maritime and Transport Technology
Delft University of Technology
Delft, Netherlands
c.loeffler@tudelft.nl

3rd Andrea Coraddu
Maritime and Transport Technology
Delft University of Technology
Delft, Netherlands
a.coraddu@tudelft.nl

4th Henk Polinder
Maritime and Transport Technology
Delft University of Technology
Delft, Netherlands
h.polinder@tudelft.nl

Abstract—Hydrogen-based shipboard power systems (SPS) are gaining prominence as a zero-emission alternative to conventional diesel-fueled systems for reducing the carbon footprint in the maritime sector. Typical designs incorporate fuel cells (FCs) as the main power supply combined with batteries in a DC distribution network. However, the efficient coordination of power generation and storage systems with different characteristics remains a challenge, particularly in topologies with multiple parallel FCs and batteries. This aspect has received limited attention in existing research. To address this challenge, this paper presents a modular approach to the hierarchical control of power generation and storage systems. Dynamic power sharing is achieved using a decentralized strategy that employs bandwidth separation, accounting for the opposing capabilities of each device. Additionally, an energy management strategy (EMS) based on equivalent consumption minimization is realized in this modular framework using a low-bandwidth communication network. The proposed architecture's modular character allows for a flexible power system reconfiguration and extension. The methodology is showcased through simulations using a short-sea cargo vessel as a case study. The results demonstrate that the bandwidth separation ensures the operation of the different technologies within their specified bandwidths, limiting the potential degradation of the FC systems. The addition of the modular EMS shows a fuel-efficient operation of the FC-battery DC SPS and a decrease in the FCs' power gradients, and thereby their aging effect.

Index Terms—DC power distribution, energy management, fuel cells, power sharing, shipboard power system

I. INTRODUCTION

In alignment with the objectives set forth by the International Maritime Organization (IMO) to mitigate the carbon footprint of the maritime sector [1], hydrogen has emerged as a promising energy carrier. Zero emission ships (ZES) with hydrogen-based generation commonly employ a hybrid fuel cell (FC)-battery energy system, supported by a DC network and power electronics interfaces to control the power flows [2], [3]. However, the effective control and optimal utilization of diverse power generation and storage devices present an ongoing challenge for FC-hybrid ships, demanding attention to their respective characteristics [4]. In particular, FCs face specific hurdles, including limited dynamic capabilities, vulnerability to performance degradation over time, and the need for a fuel-efficient operation scheme [5], [6].

Most research studies focus on small, simplistic applications of FC-battery hybrid shipboard power systems (SPS), typically with a centralized controller [7]–[9]. However, alternative control architectures are needed for power systems with higher complexity, containing multiple generation devices and energy storage systems (ESSs). A modular control approach can support the coordination of multiple different power system components while allowing an easy expansion and reconfiguration of the topology. Furthermore, the allocation of functionalities in a control hierarchy is suitable for more complex power systems [10]. This paper proposes a modular control design for both the coordinated control and energy management functionalities. The former aims to ensure a power balance under fluctuating loads, while the latter aims to improve fuel efficiency.

The power sharing in complex DC SPS is typically achieved using droop-based control [11]–[13]. However, conventional approaches do not account for differing dynamic capabilities of the components. Hence, [14] and [15] propose a resistive-capacitive droop scheme to achieve a load-frequency separation. An inductive droop element is added in [16]. In this paper, the virtual impedance approach is adapted for the coordinated control of a FC-battery DC SPS as a modular, decentralized

method for achieving power balance and peak-shaving of the FC power output.

Current research on energy management strategy (EMS) in SPS shows a trend towards heuristic optimization and predictive control approaches [17]. Such solutions are typically implemented in a centralized controller and impose a large computational burden. Furthermore, they are designed for optimization of a given system topology and application but do not account for system extension and reconfiguration. The literature on EMSs for ZES is dominated by PI-based [7], [8], [18] and rule-based approaches [19], [20], meaning a lack of optimization-based solutions. A promising optimization-based solution originating from hybrid vehicles is the equivalent consumption minimization strategy (ECMS) [21]. ECMS is a real-time control technique that reduces a global optimization problem to an instantaneous optimization that does not require information on future states. However, the overall fuel consumption and its deviation from the global optimum is dependent on the exact design, especially the choice of equivalence factor for utilizing the ESS [22]. This paper proposes an ECMS-based EMS adapted to the modular control framework leveraging a low-bandwidth communication to determine an efficient power split between FC and ESS.

Hence, the main contributions of this paper are i) the integration of a decentralized load-frequency separation for a FC-battery SPS into a modular control framework and ii) the development of a modular ECMS-based EMS. This work first describes the topology and modeling approach for an exemplary FC-battery SPS. The methodologies for the control and energy management strategies are subsequently laid out and finally applied to the case study in numerical simulations.

II. SHIPBOARD POWER SYSTEM

The proposed methodology is suitable for all-electric ships with a mainly propulsive power demand and an FC-battery power system. Furthermore, the proposed droop-based power sharing scheme is designed for DC distribution technology and assumes full controllability of all power generation and storage devices via DCDC converters. In this section, the power system of an exemplary case vessel is introduced and the methodology for modeling and simulating the power system's main components is elaborated.

A. Case Study

The considered SPS is a FC-battery hybrid with DC distribution and electric propulsion, as shown in Fig. 1. It is equipped with four FC and two battery systems distributed over two DC buses. The load of this short-sea cargo ship is mainly propulsive, hence hotel loads are disregarded in this study. The complete energy for the ship's propulsion needs to be provided by the FCs since shore power is assumed to be unavailable. All power supplies and ESSs are interfaced to the DC bus via DCDC converters, providing highly controllable power flows. Table I displays key parameters and ratings.

TABLE I
CASE STUDY PARAMETERS

Parameter	Description	Value
V_{DC}	DC-link voltage	700 V
C_{DC}	DC-link capacity (x6)	25 mF
P_{FC}	FC power rating (x4)	325 kW
P_{bat}	Battery power rating (x2)	325 kW
E_{bat}	Battery nominal capacity (x2)	225 kWh
P_{em}	Propulsion motor rating (x2)	600 kW

B. System Modeling

The key components required for the power system simulation are the FCs, batteries, DCDC converters, the DC bus, and the propulsive load. The following section contains brief descriptions of the dynamic models for these components.

1) Fuel Cells: A simple dynamic model for proton-exchange membrane fuel cells (PEMFCs) based on manufacturer data is described in [23]. Here, the data available for the Nedstack FCS 13 XXL, a PEMFC module with a maximum output power of 13.6 kW, is used [24]. A single FC stack's modeled polarization curve and power output are displayed in Fig. 2. In order to achieve the power rating of 325 kW, as listed in Table I, one FC system is comprised of 24 modules.

The voltage efficiency and hydrogen consumption of the FC stack can be computed as defined and described in [25]. The calculation is based on a theoretically achievable cell potential derived from the lower heating value of hydrogen H_{lhv}, Faraday's constant F, and the number of elementary charges per H2-molecule $n = 2$. The efficiency of a FC is proportional to its cell potential V_{cell} and consequently also to the module's voltage V_{mod} with N_s series connected cells. Hence, the voltage efficiency is estimated as

$$\eta_{FC} = \frac{V_{cell}nF}{H_{lhv}} = \frac{V_{mod}nF}{N_sH_{lhv}} \tag{1}$$

The hydrogen consumption per cell is proportional to its cell current I_{cell}. In extension, a FC module's hydrogen use $\dot{m}_{H2}$ in g/s is derived from the total current I_{mod}:

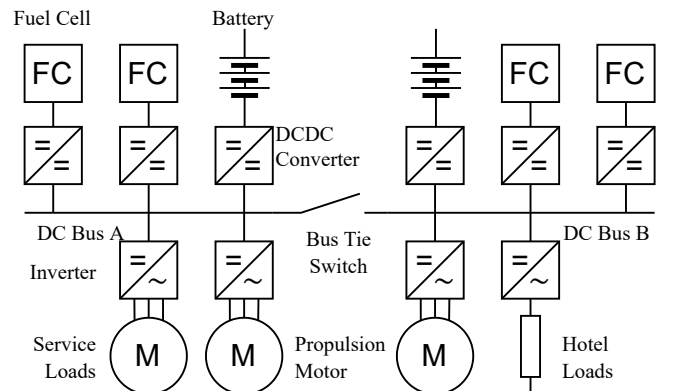$$\dot{m}_{H2} = \frac{I_{cell}N_pN_s}{F} = \frac{I_{mod}N_s}{F} \tag{2}$$

Fig. 1. Power system topology of case study

where N_p is the number of parallel connected cell stacks. Several sources compute the voltage efficiency based on the higher heating value or Gibbs free energy instead [26].

It is important to note that the voltage efficiency is idealized and neglects crossover currents, oxygen starvation, and auxiliary power consumption. Hence, the computed efficiency at low currents is unrealistically high, whereas a real FC efficiency would drop when operated at low power. For this reason, the FC operation shall be limited to the linear Ohmic loss region, as suggested in [5], while operation close to zero output power is avoided.

2) Batteries: The model reported in [27] is used for the batteries. The terminal voltage V_{bat} is obtained as

$$V_{bat} = E - R_i I_{bat} \tag{3}$$

where E is the open-circuit voltage which is dependent on the state of charge (SoC) of the battery, R_i the inner resistance, and I_{bat} the battery current. Losses occur due to the battery current through the inner resistance, yielding

$$P_{loss} = I_{bat}^2 R_i \tag{4}$$

and therefore the discharge and charge efficiencies, η_{dis} and η_{chg}, can be estimated as

$$\hat{\eta}_{dis} = \frac{V_{bat} I_{bat}}{(V_{bat} + \hat{R}_i I_{bat}) I_{bat}} \tag{5}$$

$$\hat{\eta}_{chg} = \frac{(V_{bat} + \hat{R}_i I_{bat}) I_{bat}}{V_{bat} I_{bat}} \tag{6}$$

where $\hat{R}_i$ is the estimate of R_i. Note that I_{bat} is negative when charging the battery.

3) DCDC Converters: The DCDC converters, interfacing both the battery and FC systems to the DC bus, are modeled as half-bridges, as implemented in [28]. This topology allows bi-directional power flows. However, the operation of FCs is limited to positive power flows into the DC bus. Since this work focuses on energy management and power sharing, the high-frequency switching actions of the transistors can be neglected. Hence, the converters are implemented as averaged
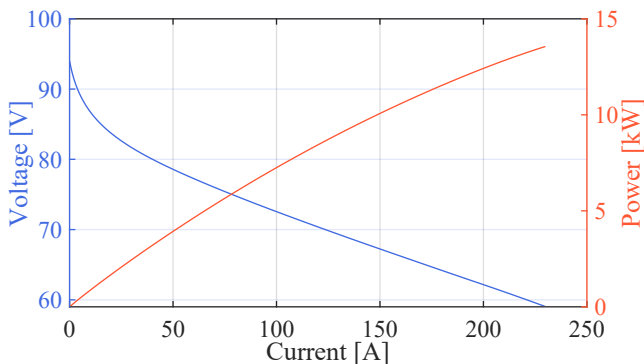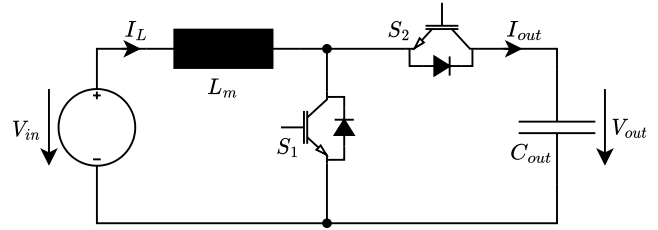

Fig. 3. Equivalent circuit of ideal half-bridge DCDC converter

models, as in [29] and [30]. The equivalent circuit of the ideal half-bridge is shown in Fig. 3. The dynamics of the averaged inductor current I_L in this topology can be computed as

$$\frac{dI_L}{dt} = \frac{1}{L_m}(V_{in} - (1 - D)V_{out}) \tag{7}$$

where V_{in} and V_{out} signify the source and output voltages, with $V_{in} < V_{out}$ and L_m the main inductance. $D \in (0, 1)$ is the duty cycle of switch S_1, serving as the control input. In the considered topology, the converter is directly interfaced to the DC bus so that V_{out} equals the DC-link voltage V_{DC}.

4) DC Bus and Loads: Transmission losses and impedances are neglected in this work due to the small scale of the SPS and the close vicinity of all components. The DC bus is modeled as a DC-link capacity C_{DC} equaling the sum of the output capacitors of all N adjacent DCDC converters $C_{out,i}$:

$$C_{DC} = \sum_{i=1}^{N} C_{out,i} \tag{8}$$

The time-dependent power profile P_{load} is obtained as an input to the power system model. Using the DC-link voltage, the power demand can be transformed into the load current I_{load} according to

$$I_{load} = P_{load}/V_{DC} \tag{9}$$

The output current of each i-th converter connected to the bus can be denoted as $I_{out,i}$. The time derivative of the DC-link voltage $\dot{V}_{DC}$ can then be computed as

$$\dot{V}_{DC} = \frac{1}{C_{DC}}(\sum_{i=1}^{N} I_{out,i} - I_{load}) \tag{10}$$

III. HIERARCHICAL CONTROL

This paper proposes a modular control architecture that facilitates easy integration of new power system components and a reconfiguration of the system's topology with minimal effort. For this purpose, the power sharing functionality is designed with a decentralized control architecture. In addition, the control strategy utilizes a central controller and a low-bandwidth communication network to enable global awareness of key variables. However, all relevant computations for determining the power reference shall be situated in the local controller so that they can be parameterized according to the respective source's characteristics. Furthermore, this architecture adds to the system's resilience against faults in the central controller and the communication network.
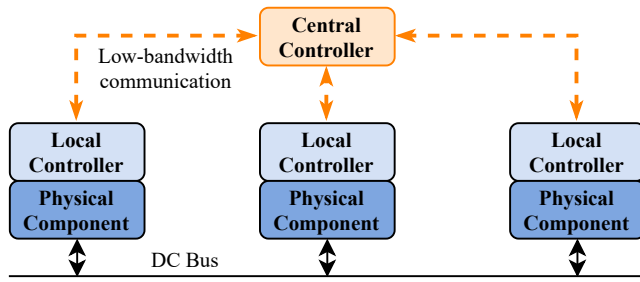

Fig. 2. Polarization curve and power output of simulation model for Nedstack FCS 13 XXL module

Fig. 4. Modular control architecture

Fig. 6. Bode plots for resistive and resistive-capacitive and resistive inductive droop schemes with corner frequency $f_c = 0.1$ Hz

A. Coordinated Control

The methodology for achieving dynamic power sharing and voltage regulation through coordinated control is based on the work presented in [16]. The authors adapted the resistive-capacitive droop approach from [14] and [15] in order to achieve a coverage of high-frequency load components with the batteries, while the FCs' power is adapted slowly. Hence, all components are operated according to their characteristics. Fig. 5 shows the virtual impedance-based droop scheme using resistive and capacitive elements. The governing equations for the droop schemes are the following:

$$\frac{I_{d,RC}}{\Delta V} = \frac{sC_{d,RC}}{sR_{d,RC}C_{d,RC} + 1} \tag{11}$$

$$\frac{I_{d,RL}}{\Delta V} = \frac{1}{R_{d,RL} + sL_{d,RL}} \tag{12}$$

where $I_{d,x}$ is the reference current for the droop-controlled source, $R_{d,x}$, $C_{d,x}$ and $L_{d,x}$ the virtual impedance elements, C_{DC} the DC bus capacity, and ΔV the error between the reference and actual DC bus voltages. Fig. 6 shows Bode plots for the virtual impedance schemes and the conventional resistive droop. It can be noted that the resistive-capacitive droop serves as a high-pass filter, while the resistive-inductive approach is a low-pass filter. Both can be tuned so that the cutoff frequencies match the characteristics of each respective component. This paper proposes using a resistive-inductive droop for the FCs' output, whereas a resistive-capacitive
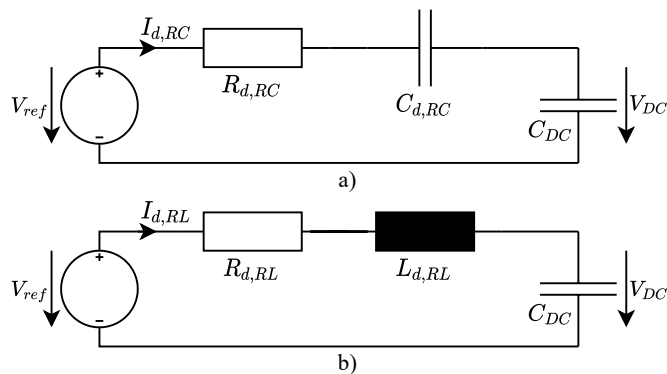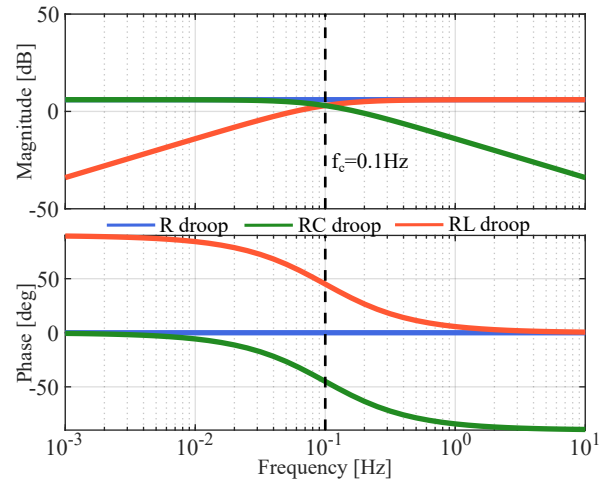

Fig. 5. Virtual impedance control with a) resistive droop, b) resistive-capacitive droop

droop is used for the batteries. In the shown example, the corner frequency f_c is chosen so that the ESS balances load frequencies above 0.1 Hz and the FCs provides the power for slower dynamics.

The described strategy using a constant reference $V_{DC,ref}$ for the DC bus voltage results in a steady state voltage error when the system is under load. To mitigate this, the reference voltage in the droop controllers, $V_{d,ref}$ is adjusted by an integral action on the voltage deviation. With V_{DC} being the actual DC bus voltage and using an integration constant on the voltage error k_V, the reference is computed as

$$V_{d,ref} = V_{DC,ref} + k_V \int V_{DC,ref} - V_{DC} dt \tag{13}$$

B. Energy Management

The ECMS concept assigns an equivalent fuel consumption value to the utilization of an ESS. An optimal power scheduling is obtained by minimizing the total fuel equivalent. In order to maintain the modular character and leverage the low-bandwidth communication, this work proposes a balancing of all components' efficiencies. This work proposes to achieve this by adding current reference I_{eta} to the output of the RC droop controller of the local battery controllers. This shifting of the battery current requires the FC controllers to adjust their output power to stabilize the DC bus voltage. Hence, an increased battery power causes the FC output to decrease, which increases the FC efficiency, and vice versa. The battery current reference, determined by the local controllers, is computed by extending (11:

$$I_{bat} = (V_{d,ref} - V_{DC})\frac{sC_{d,bat}}{sR_{d,bat}C_{d,bat} + 1} + I_{eta} \tag{14}$$

$R_{d,bat}$ and $C_{d,bat}$ are the tunable droop parameters of the local battery controller. The current reference for the FCs is computed analogously based on 12.

All components i broadcast their estimated efficiency $\eta_{est,i}$. The central controller computes and broadcasts the average

efficiency value η_{avg} to all local controllers. The efficiency estimate of hydrogen FCs can be directly derived from their output voltage as outlined in Section II-B1. For the batteries, an equivalence factor s_0 is defined, as reported in [31], initially set equal to the efficiency of the FC systems at rated power $\eta_{FC,r}$. The charging of a battery is beneficial if the equivalence factor is less than the average system efficiency discounted by the charge-discharge efficiency if

$$s_0 \leq \eta_{chg}\eta_{dis}\eta_{avg} = \eta_{chg}^2\eta_{avg} \tag{15}$$

Here, η_{chg} and η_{dis} are the current-dependent charge and discharge efficiencies, which are assumed equal. The right-hand side of (15) signifies the charge-discharge cycle efficiency for energy generated at a given system efficiency.

Analogously, the discharge of the battery is beneficial in case the equivalence factor discounted by the discharge efficiency exceeds the average system efficiency:

$$\eta_{avg} \leq s_0\eta_{chg} \tag{16}$$

The equivalent battery efficiency is estimated depending on its operating mode and the conditions formulated in 15 and 16. The current reference I_{eta} in the battery controllers is continuously updated using this estimate:

$$\eta_{bat,est} = \begin{cases} s_0\eta_{chg}, & I_{eta} > 0 (discharge) \\ s_0/\eta_{chg}^2, & I_{eta} < 0 (charge) \\ s_0, & I_{eta} = 0 \end{cases} \tag{17}$$

$$I_{eta} = k_{eta}(\gamma\eta_{bat,est} - \eta_{avg}) \tag{18}$$

where k_{eta} is a proportional factor and γ an SoC-dependent factor introducing a bias towards battery charging at low SoC and vice versa. In order to contain the energy management functionality within a realistic operation band and avoid undesired effects in off-design conditions, the local battery controller limits the received average efficiency to a minimum and maximum efficiency, η_{min} and η_{max}, so that $\eta_{avg} \in [\eta_{min}, \eta_{max}]$ and $s_0 = (\eta_{min} + \eta_{max})/2$. The factor γ shall be selected so that the current reference $I_{eta} \geq 0$ when the SoC reaches its minimum allowable value SoC_{min} and consequently $I_{eta} \leq 0$ at maximum charge SoC_{max}. In this work, γ is computed according to:

$$\gamma = 1 + \left(\frac{\eta_{max}}{s_0} - 1\right)\left(\frac{2(SoC_{est} - SoC_{ref})}{SoC_{max} - SoC_{min}}\right)^\alpha \tag{19}$$

where $SoC_{ref} = (SoC_{min} + SoC_{max})/2$ is the reference SoC, and α is a shape factor for γ. Typical limits for the battery SoC are 20 % and 80 %, as reported in [28]. Fig. 7 shows the shape of γ for varying α. The complete local control strategy for a battery system is shown in Fig 8.

IV. SIMULATION RESULTS

Measurements of the propulsive power taken during the operation of the short-sea cargo vessel are used as simulation inputs to assess the performance of the proposed modular control strategy. Even though the measurements originate from a diesel direct-drive topology, applying the obtained load
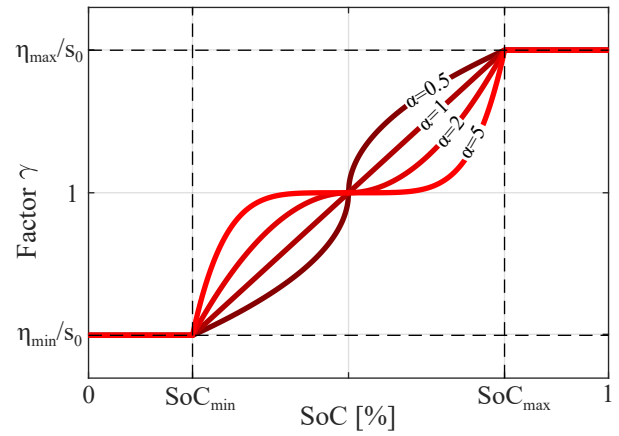

Fig. 7. Factor γ over SoC-range for different shape factors α

profile to an electric propulsion system showcases the ability of the FC-battery hybrid system to match the dynamic power of the reference vessel as a minimum requirement.

Key performance indicators for the simulations are the DC bus voltage deviation, the FC output power variation as a proxy for its lifetime degradation, and the overall fuel efficiency. Furthermore, the effectiveness of the proposed control strategy in managing the SoC of parallel ESSs is assessed.

A. Test Scenario

The operation profile of short-sea cargo vessels is steady during most of the operation time in which the ship is cruising in open water. Fast power fluctuations, e.g., due to the effect of waves, are intended to be compensated with the batteries via the load frequency decoupling in the coordinated control strategy. However, the energy management strategy can not have much effect in steady conditions since the average power needs to come from the FCs due to the limited capacity of the batteries. For this reason, a 24-hour operation profile measured
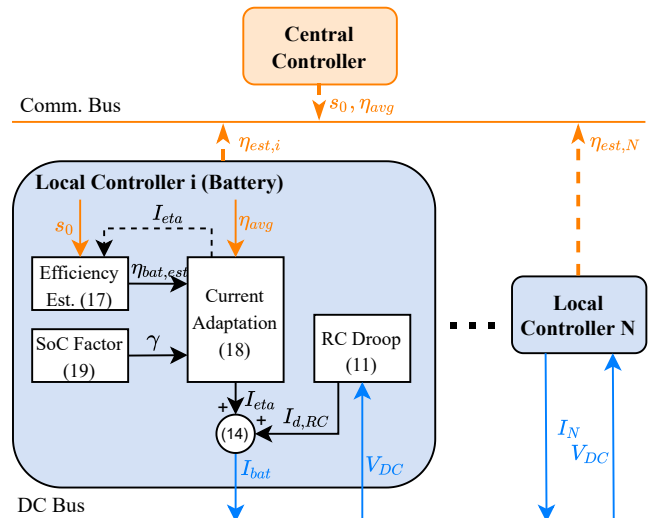

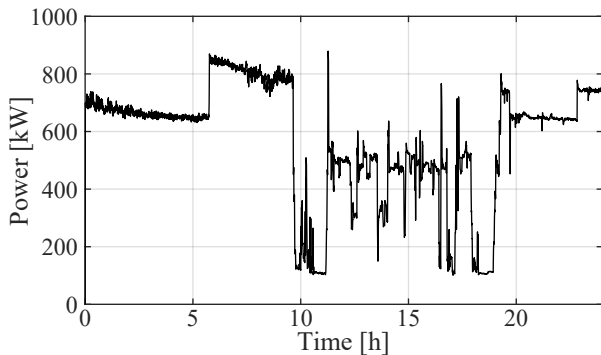Fig. 8. Adaptive droop scheme in the local controller of a battery module

Fig. 9. Load profile used for evaluation of control strategies

Fig. 10. Power sharing between FC and battery system using the benchmark control strategy without dedicated EMS

at a rate of $1\,\mathrm{Hz}$ with highly fluctuating power demands is selected in order to assess the proposed methodology. The obtained time series of the power demand is depicted in Fig. 9.

B. Theoretic maximum efficiency

To establish a reference value for the fuel consumption, it is assumed that all FCs can be operated at a constant output matching the average power demand. In practice, this is not feasible since this strategy neglects the limited capacity of the ESS and assumes that the average power demand is known. Theoretically, this operation strategy yields a minimal hydrogen consumption since the FC systems have a strictly decreasing efficiency over their operation range.

The load profile shown in Fig. 9 has an average power demand of $571\,\mathrm{kW}$ for a duration of $86\,400\,\mathrm{s}$, equaling a required energy of $13.7\,\mathrm{MWh}$. Hence, each of the FC modules needs to operate constantly at $142.75\,\mathrm{kW}$, where their voltage efficiency is $63.57\,\%$. The total amount of hydrogen needed is $655.56\,\mathrm{kg}$, which is the minimum achievable fuel consumption for this specific load profile and power system.

C. Operation without Energy Management

In order to quantify the added benefit of the EMS, the methodology described in [16] with no dedicated EMS is used as a reference. For the frequency decoupling between FCs and batteries, a time constant of $\tau_{fd} = 10\,\mathrm{s}$ is used. This matches the assumed response time of the FC systems of $10\,\mathrm{s}$, as reported in [23], so that the FC are operated to their maximum dynamic capabilities in this scenario. The resulting power sharing between FCs and batteries is depicted in Fig. 10. The battery is deployed only for providing high-frequency load changes. Accordingly, their peak power is comparably low and the depth-of-discharge is less than $1\,\%$), hence the SoC stays level. The total hydrogen consumption in this scenario amounts to $671.77\,\mathrm{kg}$ (scenario 1 in table II).

D. Fixed Equivalence Factor

The coordinated control strategy alone leads to a minimal utilization of the batteries, leaving ample capacity to be dispatched by the EMS. It is expected that the effect of the proposed EMS is highly influenced by the amount of usable
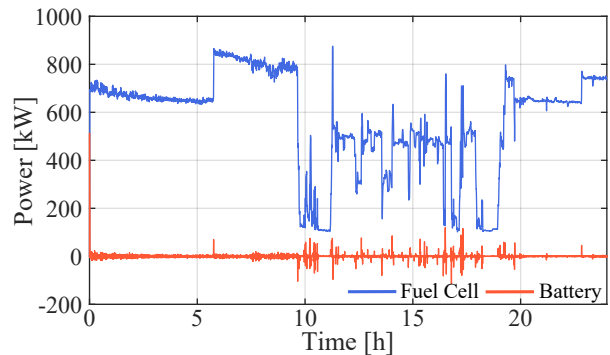
battery capacity. The control strategy is simulated multiple times with varying SoC limits. The EMS is tested in three scenarios with an allowable depth-of-discharge of $20\,\%$, $40\,\%$, and $60\,\%$, denoted as scenarios 2, 3 and 4, respectively. The utilization of the FC systems during the different scenarios is depicted in Fig. 11, and key performance indicators are listed in table II. The curves show that the FC power output is smoothed and the higher the allowed battery capacity, the longer the FCs can be operated in a more desirable operation point than matching the demand. It can further be observed that the operation strategy mostly exploits the SoC limits to their full extent. Whereas the efficiency gains are quite small with $669.22\,\mathrm{kg}$ with maximum battery capacity versus $671.77\,\mathrm{kg}$ in the benchmark ($-0.4\,\%$), the results indicate that the EMS yields significantly reduced load gradients for the FCs. Hence, the EMS supports the extension of the lifetime of the cell stacks with an increasing battery capacity. The
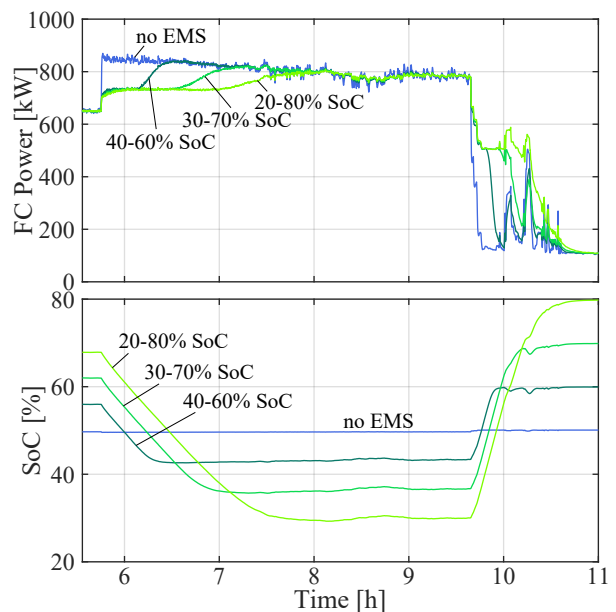

Fig. 11. Comparison of FC utilization and battery SoC for different utilization depth of the batteries

TABLE II
SIMULATION RESULTS

Scenario	1	2	3	4	5
m_{H2} [kg]	671.77	670.54	669.83	669.22	669.13
$\dot{P}_{FC,avg}$ [W/s]	701.3	429.1	407.5	398.9	393.3
$\dot{P}_{FC,rms}$ [W/s]	1443	817.9	782.7	773.1	769.2
$SoC_{bat,min}$ [%]	49.5	42.6	35.7	29.3	24.7
$SoC_{bat,max}$ [%]	50.1	60.0	69.9	79.8	78.6
$V_{DC,min}$ [V]	699.1	699.1	699.1	699.1	699.1
$V_{DC,max}$ [V]	701.0	700.9	700.9	700.9	700.9
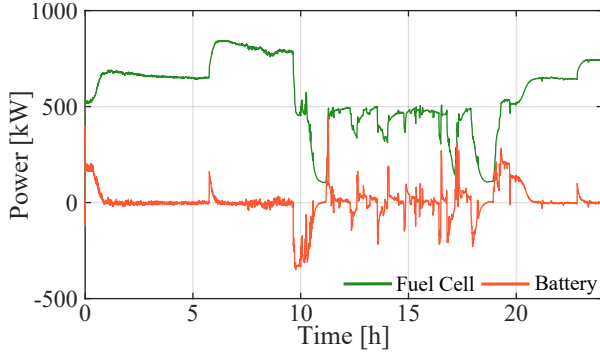
Fig. 12. Power balance and battery SoC with efficiency balancing and adaptive equivalence factor

Fig. 13. SoC management of parallel batteries

voltage reference tracking has a high accuracy in all test cases, showing that the introduction of the EMS into the modular framework does not interfere with the quality of supply. Accordingly, the results prove the applicability of the modular design for coordinated control and energy management in this work.

E. Adaptive equivalence factor

Whereas previously the equivalence factor s_0 was chosen arbitrarily, it is expected that an adaptation of s_0 can be beneficial for the efficiency. Ideally, the equivalence factor reflects the average efficiency at which the FCs generate electricity. Hence, in a fifth scenario, the equivalence factor is adapted to match the average efficiency of all FC, which approaches the overall efficiency of energy generation over a longer period. Accordingly, the equivalence factor is initialized with the efficiency corresponding to the operation of the FC at the average power of the load profile. As described previously, this yields $s_{0,init} = 63.57\,\%$. A low-pass filter on the average efficiency of all FC with a time constant of $\tau_{s0} = 10\,\mathrm{h}$ is used to let the equivalence factor slowly adapt.

The resulting power sharing between the components is depicted in Fig. 12, and results for scenario 5 are listed in Table II. Hydrogen consumption and FC power gradients are marginally improved compared to the fixed equivalence factor in scenario 4. Furthermore, the batteries are operated closer to their lower SoC limit, marking a more balanced operation of the batteries around their target charge.
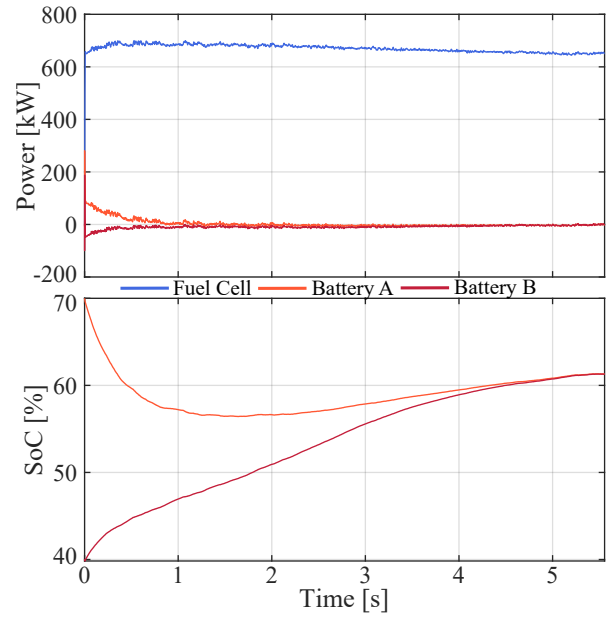
F. SoC Balancing of parallel batteries

A secondary target of the EMS is the balancing of SoC among ESS. Since γ yields an increased discharge of batteries at high SoC and discharge at low SoC, the charge of parallel batteries must converge over time. To test this, the initial SoC of the two batteries are set to $40\,\%$ and $70\,\%$, as in [16]. The power demand features low power fluctuations during its first hours, which is suitable for this investigation. The resulting battery power and SoC curves for the two batteries are displayed in Fig. 13, showing that the battery charges move towards the same value. Furthermore, the SoC balancing is sufficiently slow to not interfere with the power sharing.

V. CONCLUSION

This paper presents a modular control framework for coordinated control and energy management in a a FC-battery DC SPS.. In the proposed architecture, each local controller computes the power references based on its source's parameters. The architecture is complemented by a low-bandwidth communication network and a central controller to cater for information sharing and situational awareness.

A dynamic power sharing strategy based on a virtual impedance has proven as a useful tool to achieve a load-frequency separation between FCs and batteries so that the operation of each source matches its specific characteristics. This power sharing strategy has shown to stabilize and restore the DC bus voltage effectively around its reference value.

Moreover, the extension of this control strategy by an ECMS-based EMS was described. This study works as a proof-of-concept for the inclusion of the coordinated control and energy management functionalities within a modular control architecture. The hierarchical organization of the functionalities ensures that control objectives do not interfere

with one another. In numerical simulations of a case study, the applied EMS yields a significant reduction of FC load gradients. A marginal decrease in overall fuel consumption could furthermore be achieved at the example of an exemplary mission. Additionally, the proposed EMS has demonstrated its ability to balance the SoC of parallel ESS during a mission.

In future investigations, this modular framework can serve as a basis for the implementation of more elaborate EMS, to optimize the efficiency gains. Moreover, attention will be placed on the system extension and reconfiguration using this modular approach. It is possible to add new ESS technologies as well as different FC and battery types without changing the control architecture. In the same manner, this strategy is able to adapt to component faults by excluding them from the coordinated control. Further investigations will analyze the behavior of parallel components with differing characteristics, especially changed efficiencies, e.g., due to aging effects.

REFERENCES

[1] T.-H. Joung, S.-G. Kang, J.-K. Lee, and J. Ahn, "The IMO initial strategy for reducing Greenhouse Gas(GHG) emissions, and its follow-up actions towards 2050," *Journal of International Maritime Safety, Environmental Affairs, and Shipping*, vol. 4, no. 1, pp. 1–7, Jan. 2020.

[2] J. F. Hansen and F. Wendt, "History and State of the Art in Commercial Electric Ship Propulsion, Integrated Power Systems, and Future Trends," *Proceedings of the IEEE*, vol. 103, no. 12, pp. 2229–2242, Dec. 2015.

[3] C. Nuchturee, T. Li, and H. Xia, "Energy efficiency of integrated electric propulsion for ships – A review," *Renewable and Sustainable Energy Reviews*, vol. 134, p. 110145, Dec. 2020.

[4] L. Xu, J. Guerrero, A. Lashab, B. Wei, N. Bazmohammadi, J. Vasquez, and A. Abusorrah, "A Review of DC Shipboard Microgrids—Part II: Control Architectures, Stability Analysis, and Protection Schemes," *IEEE Transactions on Power Electronics*, vol. 37, no. 4, pp. 4105–4120, Apr. 2022.

[5] N. Shakeri, M. Zadeh, and J. Bremnes Nielsen, "Hydrogen Fuel Cells for Ship Electric Propulsion: Moving Toward Greener Ships," *IEEE Electrification Magazine*, vol. 8, no. 2, pp. 27–43, Jun. 2020.

[6] A. Haxhiu, A. Abdelhakim, S. Kanerva, and J. Bogen, "Electric Power Integration Schemes of the Hybrid Fuel Cells and Batteries-Fed Marine Vessels—An Overview," *IEEE Transactions on Transportation Electrification*, vol. 8, no. 2, pp. 1885–1905, Jun. 2022.

[7] L. Balestra and I. Schjølberg, "Energy management strategies for a zero-emission hybrid domestic ferry," *International Journal of Hydrogen Energy*, vol. 46, no. 77, pp. 38 490–38 503, Nov. 2021.

[8] H. Chen, Z. Zhang, C. Guan, and H. Gao, "Optimization of sizing and frequency control in battery/supercapacitor hybrid energy storage system for fuel cell ship," *Energy*, vol. 197, p. 117285, Apr. 2020.

[9] A. M. Bassam, A. B. Phillips, S. R. Turnock, and P. A. Wilson, "An improved energy management strategy for a hybrid fuel cell/battery passenger vessel," *International Journal of Hydrogen Energy*, vol. 41, no. 47, pp. 22 453–22 464, Dec. 2016.

[10] Z. Jin, L. Meng, J. M. Guerrero, and R. Han, "Hierarchical Control Design for a Shipboard Power System With DC Distribution and Energy Storage Aboard Future More-Electric Ships," *IEEE Transactions on Industrial Informatics*, vol. 14, no. 2, pp. 703–714, Feb. 2018.

[11] B. Zahedi and L. E. Norum, "Voltage regulation and power sharing control in ship LVDC power distribution systems," in *2013 15th European Conference on Power Electronics and Applications (EPE)*, Sep. 2013, pp. 1–8.

[12] M. U. Mutarraf, Y. Guan, Y. Terriche, C.-L. Su, M. Nasir, J. C. Vasquez, and J. M. Guerrero, "Adaptive Power Management of Hierarchical Controlled Hybrid Shipboard Microgrids," *IEEE Access*, vol. 10, pp. 21 397–21 411, 2022.

[13] Z.-X. Xiao, Y.-Z. Guan, H.-W. Fang, Y. Terriche, and J. M. Guerrero, "Dynamic and Steady-State Power-Sharing Control of High-Efficiency DC Shipboard Microgrid Supplied by Diesel Generators," *IEEE Systems Journal*, vol. 16, no. 3, pp. 4595–4606, Sep. 2022.

[14] X. Chen, J. Zhou, M. Shi, L. Yan, W. Zuo, and J. Wen, "A Novel Virtual Resistor and Capacitor Droop Control for HESS in Medium-Voltage DC System," *IEEE Transactions on Power Systems*, vol. 34, no. 4, pp. 2518–2527, Jul. 2019.

[15] J. Khazaei, "Optimal Flow of MVDC Shipboard Microgrids With Hybrid Storage Enhanced With Capacitive and Resistive Droop Controllers," *IEEE Transactions on Power Systems*, vol. 36, no. 4, pp. 3728–3739, Jul. 2021.

[16] T. Kopka, F. Mylonopoulos, A. Coraddu, and H. Polinder, "Decentralized Power Sharing with Frequency Decoupling for a Fuel Cell-battery DC Shipboard Power System," in *Modelling and Optimisation of Ship Energy Systems (MOSES)*, Oct. 2023, in press.

[17] P. Xie, J. M. Guerrero, S. Tan, N. Bazmohammadi, J. C. Vasquez, M. Mehrzadi, and Y. Al-Turki, "Optimization-Based Power and Energy Management System in Shipboard Microgrid: A Review," *IEEE Systems Journal*, vol. 16, no. 1, pp. 578–590, Mar. 2022.

[18] C.-L. Su, X.-T. Weng, and Ching-Jin Chen, "Power generation controls of fuel cell/energy storage hybrid ship power systems," in *2014 IEEE Conference and Expo Transportation Electrification Asia-Pacific (ITEC Asia-Pacific)*. Beijing, China: IEEE, Aug. 2014, pp. 1–6.

[19] J. Han, J.-F. Charpentier, and T. Tang, "An energy management system of a fuel cell/battery hybrid boat," *Energies*, vol. 7, no. 5, pp. 2799–2820, 2014.

[20] H. Pourrahmani, M. Gay, A. Yavarinasab, and J. Van herle, "Optimization and dynamic responses of an integrated fuel cell and battery system for an 800 kW ferry: A case study," *Energy Reports*, vol. 8, pp. 9757–9776, Nov. 2022.

[21] A. Sciarretta, L. Serrao, P. Dewangan, P. Tona, E. Bergshoeff, C. Bordons, L. Charmpa, Ph. Elbert, L. Eriksson, T. Hofman, M. Hubacher, P. Isenegger, F. Lacandia, A. Laveau, H. Li, D. Marcos, T. Nüesch, S. Onori, P. Pisu, J. Rios, E. Silvas, M. Sivertsson, L. Tribioli, A.-J. van der Hoeven, and M. Wu, "A control benchmark on the energy management of a plug-in hybrid electric vehicle," *Control Engineering Practice*, vol. 29, pp. 287–298, Aug. 2014.

[22] L. Serrao, S. Onori, and G. Rizzoni, "A Comparative Analysis of Energy Management Strategies for Hybrid Electric Vehicles," *Journal of Dynamic Systems, Measurement, and Control*, vol. 133, no. 3, Mar. 2011.

[23] S. N. M., O. Tremblay, and L.-A. Dessaint, "A generic fuel cell model for the simulation of fuel cell vehicles," in *2009 IEEE Vehicle Power and Propulsion Conference*, Sep. 2009, pp. 1722–1729.

[24] "Nedstack — FCS 13-XXL," https://nedstack.com/en/pem-fcs-stack-technology/fcs-13-xxl.

[25] F. Barbir and F. Barbir, *PEM Fuel Cells: Theory and Practice*. Burlington, UNITED STATES: Elsevier Science & Technology, 2005.

[26] K. W. Harrison, R. Remick, A. Hoskin, and G. D. Martin, "Hydrogen Production: Fundamentals and Case Study Summaries; Preprint," National Renewable Energy Lab. (NREL), Golden, CO (United States), Tech. Rep. NREL/CP-550-47302, Jan. 2010.

[27] O. Tremblay, L.-A. Dessaint, and A.-I. Dekkiche, "A Generic Battery Model for the Dynamic Simulation of Hybrid Electric Vehicles," in *2007 IEEE Vehicle Power and Propulsion Conference*, Sep. 2007, pp. 284–289.

[28] L. Balestra and I. Schjølberg, "Modelling and simulation of a zero-emission hybrid power plant for a domestic ferry," *International Journal of Hydrogen Energy*, vol. 46, no. 18, pp. 10 924–10 938, Mar. 2021.

[29] B. Zahedi and L. E. Norum, "Modeling and Simulation of All-Electric Ships With Low-Voltage DC Hybrid Power Systems," *IEEE Transactions on Power Electronics*, vol. 28, no. 10, pp. 4525–4537, Oct. 2013.

[30] A. Haseltalab, L. van Biert, H. Sapra, B. Mestemaker, and R. R. Negenborn, "Component sizing and energy management for SOFC-based ship power systems," *Energy Conversion and Management*, vol. 245, p. 114625, Oct. 2021.

[31] L. C. W. Yuan, T. Tjahjowidodo, G. S. G. Lee, R. Chan, and A. K. Ådnanes, "Equivalent Consumption Minimization Strategy for hybrid all-electric tugboats to optimize fuel savings," in *2016 American Control Conference (ACC)*, Jul. 2016, pp. 6803–6808.